Multicolour imaging of post-Golgi sorting and trafficking in live cells

Patrick Keller*†‡, Derek Toomre*‡, Elena Díaz*, Jamie White*§ and Kai Simons*†¶

**Cell Biology/Biophysics Programme, European Molecular Biology Laboratory (EMBL), Meyerhofstrasse 1, D-69117 Heidelberg, Germany*
†Max Planck Institute of Molecular Cell Biology and Genetics, Pfotenhauerstrasse 108, D-01307 Dresden, Germany
§Current address: Massachusetts General Hospital Cancer Center, 149-7202 13th Street, Charlestown, Massachusetts 02129, USA
‡These authors contributed equally to this work.
¶e-mail: Simons@mpi-cbg.de

The biogenesis and maintenance of asymmetry is crucial to many cellular functions including absorption and secretion, signalling, development and morphogenesis. Here we have directly visualized the segregation and trafficking of apical (glycosyl phosphatidyl inositol-anchored) and basolateral (vesicular stomatitis virus glycoprotein) cargo in living cells using multicolour imaging of green fluorescent protein variants. Apical and basolateral cargo segregate progressively into large domains in Golgi/trans-Golgi network structures, exclude resident proteins, and exit in separate transport containers. These remain distinct and do not merge with endocytic structures suggesting that lateral segregation in the trans-Golgi network is the primary sorting event. Fusion with the plasma membrane was detected by total internal reflection microscopy and reveals differences between apical and basolateral carriers as well as new 'hot spots' for exocytosis.

An important aspect of cellular asymmetry is cell-surface polarity created by the formation of discrete regions of different protein and lipid composition[1,2]. Physical barriers can help segregate these domains: tight junctions separate apical and basolateral domains in epithelial cells; the axon hillock performs a similar function in neurons[3,4]. However, such barriers are not prerequisite for asymmetry as migratory cells also display a specific subset of proteins at the leading edge during locomotion[5]. The formation of discrete regions of different composition, and thus the generation of cell-surface polarity, involves the sorting of different classes of protein and lipid to distinct physical regions[1,2,6]. These sorting events can occur either during initial delivery of newly synthesized material, or after delivery by a transcytotic route[7]. Biochemical evidence suggests that non-polarized cells are capable of sorting newly synthesized cargo into different containers before surface delivery[8,9]. Post-Golgi sorting is emerging as a principal mechanism for generating cellular polarity[10].

At the molecular level, exocytic sorting of membrane proteins relies on different hierarchical sorting signals, which target proteins to apical and basolateral domains in epithelial cells. Similar sorting signals appear to function in many cell types including non-polarized cells[11]. Consistent with earlier nomenclature[8,9] we will refer to these as 'apical' and 'basolateral' pathways even though we are not strictly referring to polarized epithelial cells. Basolateral targeting of proteins is often mediated by hydrophobic tyrosine or dileucine motifs in the cytoplasmic tail that resemble, but are distinct from, internalization motifs[12]. Little is known about the basolateral sorting machinery, although evidence indicates that at least some of these determinants are recognized by adaptor protein 1 (AP-1) adaptors containing the μ1B subunit[13]. In contrast, apical proteins have transmembrane or luminal sorting motifs[14]. In particular, *N*- and *O*-linked oligosaccharides can act as apical targeting signals[15]. Here, too, a detailed mechanism of sorting is lacking, but cumulative evidence suggests that apical cargo is sequestered into glycosphin-

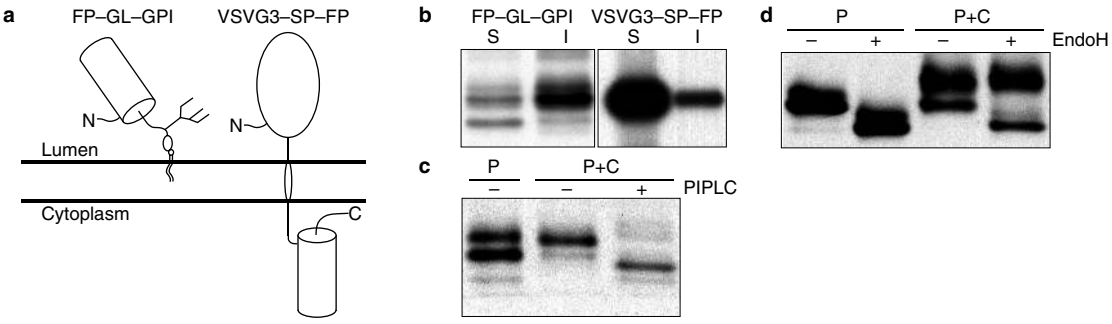

Figure 1 **Biochemical characterization of fluorescent apical and basolateral cargo in MDCK cells. a**, FP–GL–GPI is a GPI-anchored protein containing an ER-import signal, FP, and a consensus *N*-glycosylation (GL) site fused to a GPI-attachment signal. VSVG3–SP–FP is based on VSVG3–FP[21], and differs from it by having a longer spacer (SP) between VSVG and FP. **b**, Detergent extraction revealed that FP–GL–GPI was mainly Triton X-100 insoluble, whereas VSVG3–SP–FP was mainly soluble. **c**, Proper addition of the GPI-anchor was ascertained by PIPLC treatment. In the ER (P) the GPI-anchor was added to the precursor (lower band) yielding the upper band. In post-ER compartments (P+C), this species was predominant and fully sensitive to PIPLC treatment. **d**, The *N*-glycosylation site in FP–GL–GPI is used. EndoH digestion showed that FP–GL–GPI was fully sensitive in the ER, and the species containing the GPI-anchor became insensitive after exiting the ER.

© 2001 Macmillan Magazines Ltd

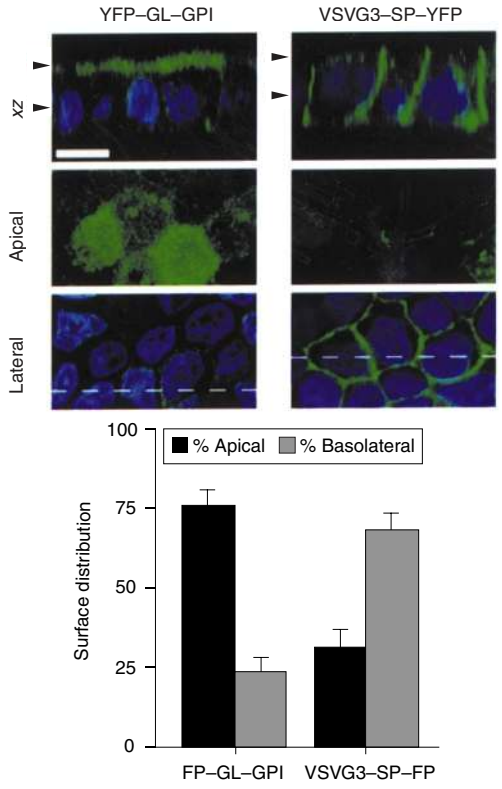

Figure 2 **Surface distribution in polarized MDCK cells.** Filter-grown MDCK cells were infected with adenoviruses expressing FP fusions. After an overnight incubation, protein synthesis was inhibited with cycloheximide and the cells were fixed 1 h later for confocal microscopy (top). Alternatively, the surface distribution (n = 7) was analysed using domain-specific surface biotinylation (bottom). Representative *xy* sections for apical and lateral domains are shown. Their positions with respect to the monolayer are indicated by arrowheads in the *xz* section. The position from where the *xz* section was taken is indicated in the lateral panel by the dashed line. Nuclei were stained with Hoechst 33342. Scale bar, 10 μm.

golipid-cholesterol-rich domains, or rafts, in the trans-Golgi network (TGN)[16].

At the cellular level, it remains to be seen how and where the molecular mechanisms of exocytic sorting first generate physically separate regions of distinct composition, ultimately manifested as the apical and basolateral surfaces of polarized cells. Early studies, using virus infected cells and biochemical or immuno-electron microscopy approaches, showed that apical and basolateral cargo trafficked together through a common Golgi complex, but arrived on opposite plasma membrane domains in MDCK cells[17–19]. In a post-Golgi region, presumably the TGN[19], the markers separated and were believed to traffic in small vesicles directly to the plasma membrane.

It has since become clear from studies in live cells of green fluorescent protein (GFP) fused to markers of the biosynthetic pathway that a significant proportion of exocytic cargo can be transported from the Golgi in large, pleiomorphic, tubulovesicular transport containers (TCs) as well as small vesicles[20–23]. However, these single-colour studies could not address how or where the dynamic process of apical/basolateral sorting occurs.

Here we have used multicolour imaging to analyse directly the cellular mechanisms and sites of apical/basolateral sorting in living cells. GFP colour variants (cyan, CFP; yellow, YFP)[24] were used to generate fluorescent exocytic cargo, as well as Golgi and TGN resident proteins. Adenovirus-mediated expression led to efficient co-expression of these markers, and fast dual colour fluorescence microscopy allowed visualization with high temporal and spatial resolution. We visualized sorting in both polarized and non-polarized cells, determined the site of sorting by monitoring exocytic cargo with respect to Golgi, TGN and endocytic markers, and using total internal reflection (TIR) microscopy analysed fusion of cargo with the plasma membrane.

Results

Characterization of apical and basolateral cargo. To analyse segregation of apical and basolateral cargo in living cells, we constructed both cyan and yellow fluorescent protein (FP) fusions (Fig. 1a) designed to be transported apically or basolaterally in polarized cells. As an apical marker, we generated a glycosyl phosphatidyl inositol (GPI)-anchored version of FP, FP–GL–GPI, which is also *N*–Glycosylated (GL) (Fig. 1c, d). As a basolateral marker, we used a fusion of the ts045-temperature-sensitive mutant of vesicular stomatitis virus glycoprotein, VSVG, and FP. A spacer (SP) between VSVG and FP was added to yield VSVG3–SP–FP, which allowed the basolateral targeting determinant to be recognized (P.K., unpublished).

To verify that our live cell markers behaved appropriately as raft and non-raft proteins, we determined their insolubility in the non-ionic detergent Triton X-100 on ice. As expected, the apical marker was 73% insoluble, whereas the basolateral marker was only 6% insoluble (Fig. 1b). Confocal microscopy analysis showed predominately apical localization of FP–GL–GPI and lateral localization of VSVG3–SP–FP in fully polarized MDCK II cells (Fig. 2). Biochemical studies using surface biotinylation supported these results and revealed that FP–GL–GPI was 76.1 ± 5.1% apical. In contrast, VSVG3–SP–FP was 68.5 ± 5.5% basolateral (Fig. 2). Although this sorting is not perfect, it is comparable with that of the non-tagged VSVG protein in MDCK II cells, which sort VSVG less efficiently than MDCK I cells (our unpublished observation). Thus, the bulk of our apical and basolateral fluorescent probes were correctly sorted and targeted in MDCK II cells.

Table 1 Basolateral post-Golgi TC's do not traverse endocytic structures

	Cells*	Exocytic cargo only†	Endocytic cargo only†	Exocytic + endocytic cargo‡ (total/moving)§
VSVG3–SP–YFP + Texas-Red-transferrin	5	69	155	5/1 (6.7/1.4%)¶
VSVG3–SP–YFP + Texas-Red-dextran	4	64	149	5/0 (6.7/0%)¶

* Number of cells analysed.
† Number of structures positive for either exocytic or endocytic cargo.
‡ Number of structures positive for both exocytic or endocytic cargo.
§ Total/moving describes the the total number of overlapping structures and the number of these that are moving over time.
¶ Per cent of VSVG3–SP–YFP structures that coincide with endocytic markers.

© 2001 Macmillan Magazines Ltd

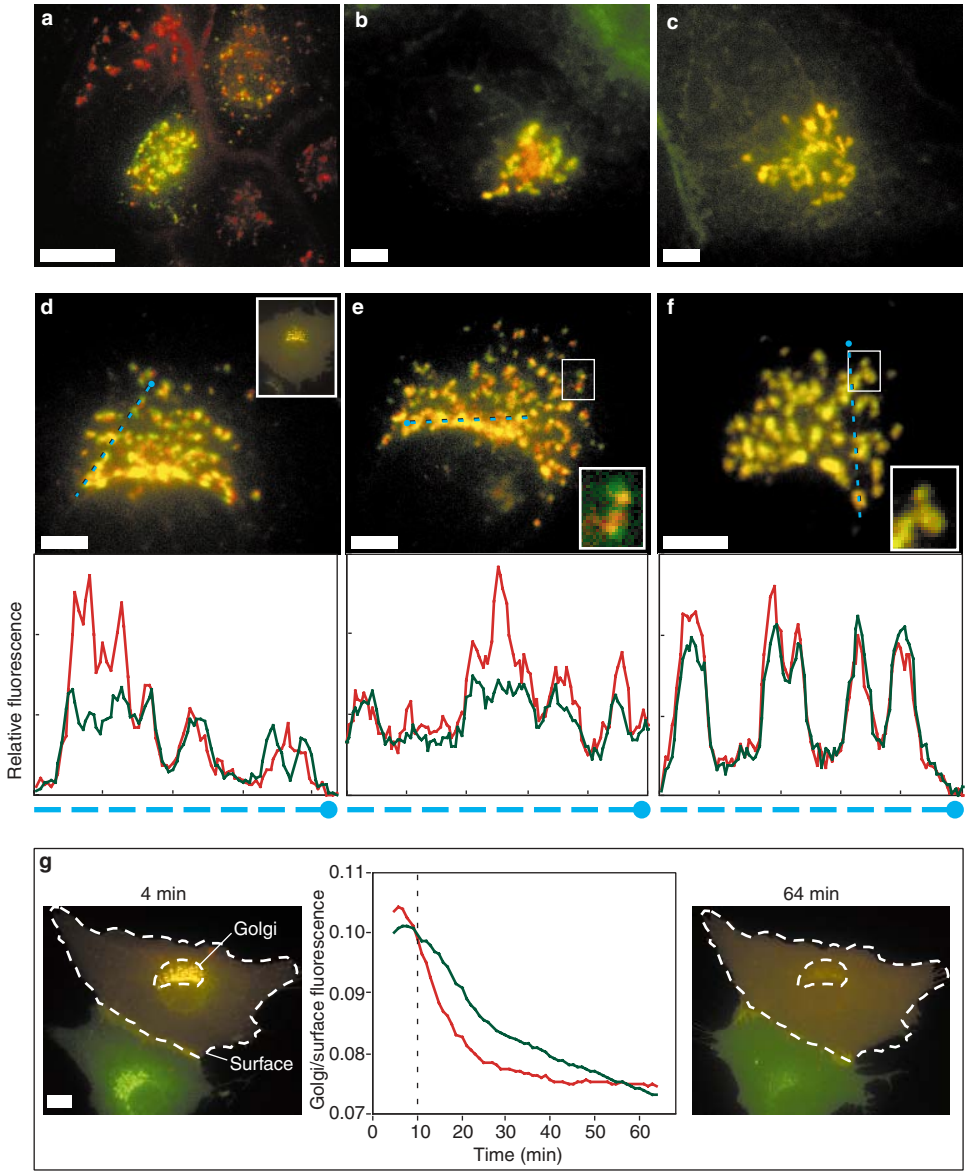

Figure 3 **Apical and basolateral cargo segregate in the Golgi of polarized MDCK and non-polarized PtK$_2$ cells.** See also Supplementary Information. **a**, Filter-grown MDCK cells were infected with adenoviruses expressing YFP–GL–GPI (red) and VSVG3–SP–CFP (green). After a 19.5 °C block for 2 h, cargo was released from the Golgi for 5 min at 37 °C, and the cells were fixed. A brightest point projection through a stack of acquired images is shown. **b**, **c**, Alternatively, after a 19.5 °C block, living double-infected MDCK cells grown on glass coverslips were imaged at 37 °C so that the Golgi region was in focus. A single image taken 5 min after release from the Golgi block is shown for cells double infected with VSVG3–SP–YFP (red) and CFP–GL–GPI (green) (**b**), and for YFP–GL–GPI (red) and CFP–GL–GPI (green) (**c**). **d**, A living PtK$_2$ cell expressing VSVG3–SP–YFP (red) and CFP–GL–GPI (green) imaged 7 h after infection without any temperature block shows segregation of apical and basolateral cargo in the Golgi. Insert, the whole cell; dashed blue line indicates where the representative intensity profiles were obtained (see Methods). **e**, **f**, PtK$_2$ cells expressing VSVG3–SP–YFP (red) and CFP–GL–GPI (green) (**e**) or YFP–GL–GPI (red) and CFP–GL–GPI (green) (**f**). After a 19.5 °C block for 2 h, cargo was released from the Golgi for 10 min at 37 °C, and the cells were fixed. To help illustrate the respective segregation and overlap, typical enlarged areas and two-colour intensity profiles across the Golgi are displayed. **g**, CFP–GL–GPI (green) and VSVG3–SP–YFP (red) were followed over time to analyse the kinetics of Golgi exit, and the relative ratio of fluorescence in the Golgi and the plasma membrane was quantitated (see Methods). Note that segregation of cargo in the Golgi is not visible at this magnification. Scale bars, 5 μm (**a–f**); and 10 μm (**g**).

Apical and basolateral cargo segregate within the Golgi. To address where sorting occurs along the exocytic pathway, we expressed both markers in filter-grown MDCK cells using adenoviruses. Differently coloured apical and basolateral cargo were accumulated in the Golgi at 19.5 °C for 2 h, released 5 min at 37 °C and fixed. To evaluate the distribution of both proteins throughout the entire volume of columnar MDCK cells, we acquired serial optical sections, deconvolved the data and generated 3D projections (Fig. 3a; and Supplementary Information movie). We observed a partial separation of apical and basolateral cargo in the Golgi region. This separation was also observed in living partially polarized MDCK cells (Fig. 3b; and Supplementary Information movie), which spread over a larger area than the corresponding fully polarized cells. The observed segregation was not due to differential changes of fluorescent properties of CFP and YFP, for example caused by pH changes

© 2001 Macmillan Magazines Ltd

articles

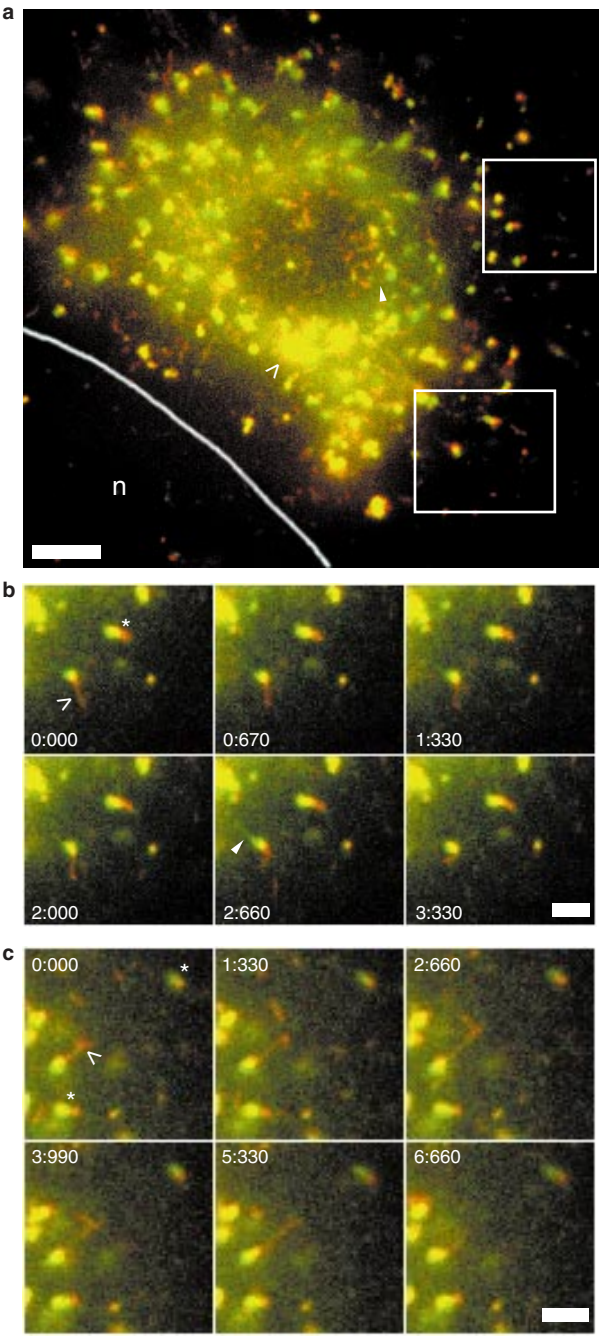

Figure 4 **Dynamics of cargo segregation in the Golgi of live cells.** See also Supplementary Information. PtK_2 cells were infected with adenoviruses expressing VSVG3–SP–YFP (red) and CFP–GL–GPI (green). **a**, A frame of a movie taken 20 min after release from the 19.5 °C block. Some regions showed extensive cargo overlap (>), whereas others showed strong segregation (arrowhead). The nucleus (n) is indicated. (**b**) and (**c**) are enlargements of the areas boxed in (**a**) and show individual frames. The time relative to the first image is shown in s:ms. Structures stably segregated cargo over time (*) and tubular structures containing VSVG3–SP–YFP (>) emerged from structures which contained both cargo. Notably, a CFP–GL–GPI tubule emerged simultaneously with a VSVG3–SP–YFP tubule from the same structure (**b**; arrowhead in 2:660). Scale bars, 5 μm (**a**); and 2 μm (**b**, **c**).

along the exocytic pathway, because YFP–GL–GPI and CFP–GL–GPI completely overlapped (Fig. 3c; and Supplementary Information movie). Further studies in live, fully polarized filter-grown MDCK cells were not possible with acceptable time resolution as most of the cargo trafficked rapidly along the *z* axis.

We therefore continued our analysis in PtK_2 cells. These non-polarized cells are very flat and most of the separation and trafficking events occur in a single *xy* plane[22]. This also allowed us to test whether, as biochemical studies have indicated[8,9], several exocytic pathways occur in non-polarized cells. In living cells imaged 7 h after infection, we observed a partial segregation of apical and basolateral cargo in the Golgi as exemplified by the intensity profiles (Fig. 3d); however, under these conditions only a small fraction of cargo is in the Golgi (Fig. 3d, insert). This weak Golgi fluorescence, which required longer exposure times and was quickly photobleached, made more extensive time-lapse imaging impracticable.

To improve the fluorescence signal, we accumulated cargo in the Golgi by a 19.5 °C block. Cells were released from the temperature block and fixed after 10 min. Apical and basolateral cargo segregated into large domains within the Golgi region (Fig. 3e), as in cells never blocked at 19.5 °C (Fig. 3d). In contrast, YFP–GL–GPI and CFP–GL–GPI colocalized almost completely as observed by the high degree of overlap in the intensity profiles through the Golgi (Fig. 3f). The fact that apical/basolateral cargo only partially segregated is not surprising since after a 10 min release from the temperature block only a small per cent of cargo has exited the Golgi. This is shown by the relative kinetics of cargo exit (Fig. 3g, middle panel, dashed line), consistent with other reports[20,22]. Quantitation of thresholded projections also showed significant differences in apical/basolateral cargo (data not shown).

Dynamics of cargo segregation in the Golgi of live cells. Apical and basolateral cargo were expressed in PtK_2 cells, incubated without a previous endoplasmic reticulum (ER) block at 19.5 °C to accumulate cargo in the Golgi, and visualized live at various times after shifting to 37 °C. Consistent with our results in fixed cells, we observed distinct separation of apical and basolateral cargo in Golgi regions (Fig. 4a).

In some regions, separation was extensive: Golgi structures contained predominately one type of cargo. Movies of segregation dynamics showed that the two types of cargo initially overlapped in a single Golgi structure, but then separated over time to form stable domains. These domains exhibited complementary dynamics, suggesting they were regions of the same structure. Transport containers containing exclusively one type of cargo frequently exited from these domains. Occasionally we also saw two tubules, one containing basolateral and the other apical cargo, simultaneously emerging from the same globular structure (Fig. 4b). As in fixed cells, YFP and CFP apical fusion proteins did not separate significantly (data not shown). Together, these results suggest that apical and basolateral cargo first laterally segregate into large dynamic domains, and later exit the Golgi in separate TCs.

Cargo progresses from the Golgi stack to the TGN before exit. To define the site of cargo segregation more accurately, we first analysed Golgi organization in living PtK_2 cells. We compared the Golgi stack marker, GalNAc transferase II fused to FP (T2–FP)[25,26] with a TGN marker, TGN38–FP[27]. They were juxtaposed, yet primarily separate (Fig. 5a; and Supplementary Information movie), consistent with the known localization of the endogenous proteins[25–27]. We then analysed the distribution of our basolateral marker with respect to T2–FP or TGN38–FP during passage of a synchronous pulse of cargo through the Golgi complex. 15 min after release from the ER, VSVG3–SP–YFP colocalized with T2–CFP, with no apparent separation before colocalization. Thereafter, regions containing basolateral cargo were organized rapidly into separate domains from which TCs exited. The dynamics observed suggested lateral segregation of cargo and resident, within a Golgi element. Over time, domain formation led to an overall polarization of cargo within the Golgi, similar to the separation of TGN and Golgi residents, and so most probably represented entry into the TGN (Fig. 5b; and Supplementary Information movie). In contrast, VSVG3–SP–CFP and TGN38–YFP first localized to adjacent yet pri-

© 2001 Macmillan Magazines Ltd

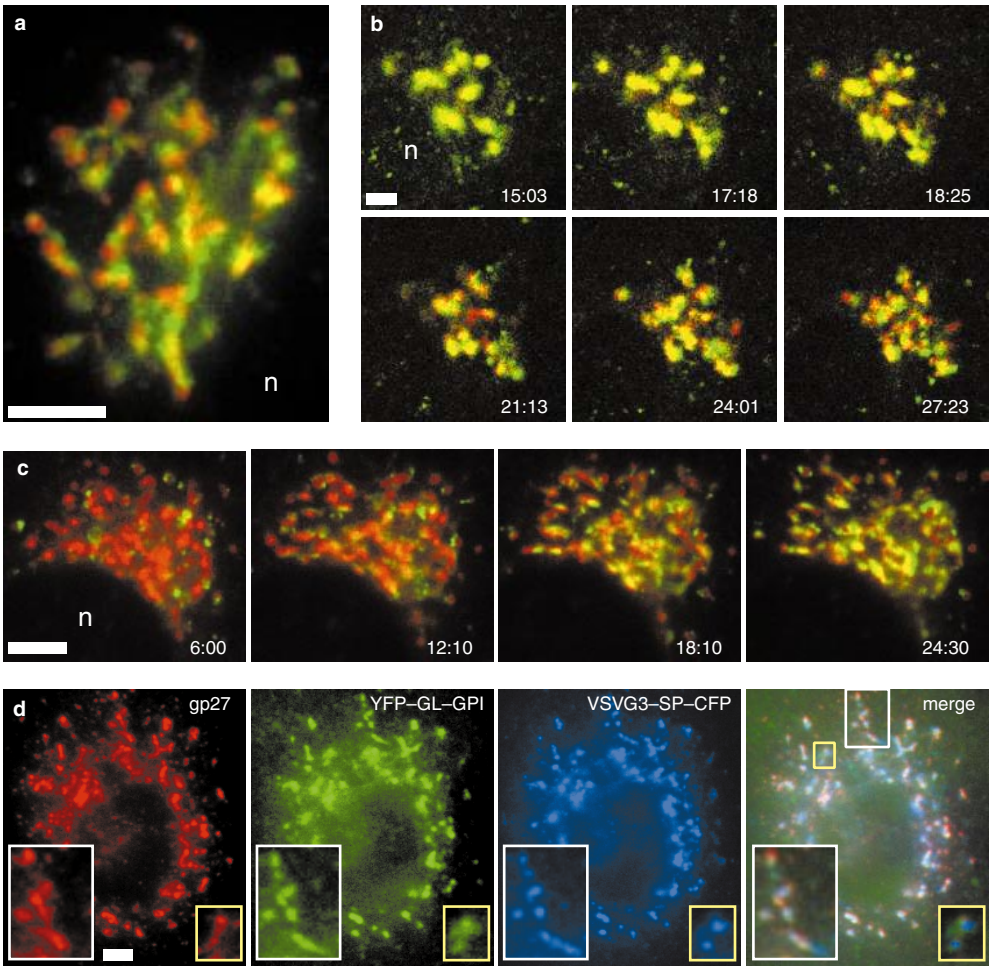

Figure 5 **Cargo progresses from the Golgi stack to the TGN before exit.** See also Supplementary Information. **a**, Brightest point projection of the Golgi region of a PtK_2 cell transiently transfected with TGN38–YFP (red) and T2–CFP (green). **b**, Individual frames from a movie of a cell expressing VSVG3–SP–YFP (green) and T2-CFP (red), 15 min after VSVG3–SP–YFP had been released from the ER. The time is shown in min:s. Cargo changed distribution as the Golgi emptied. T2–CFP and cargo overlapped extensively at the beginning, but segregated by the end of the sequence. **c**, Images from a cell expressing TGN38–YFP (red) and VSVG3–SP–CFP (green) after VSVG3–SP–CFP had been released from the ER. Initially, cargo and TGN38–YFP were separate, but cargo then moved into TGN38–YFP-positive structures. **d**, Immunofluorescence for the Golgi marker gp27 (red) on a cell expressing YFP–GL–GPI (green) and VSVG3–SP–CFP (blue). Individual channels and a merge are shown. Boxed areas are enlarged twofold. The nucleus (n) is indicated. Scale bars, 5 μm (**a**, **c**, **d**); and 2 μm (**b**).

marily separate elements and then colocalized (Fig. 5c). At later times, there was still a partial segregation which probably reflects cargo exiting the TGN.

To establish further whether segregation occurred within the Golgi/TGN or later in peripheral TCs, we performed triple-colour immunofluorescence using antibodies against the Golgi protein gp27 (ref. 28), along with YFP- and CFP-labelled cargo. Notably, domains in which apical and basolateral cargo were segregated overlapped to a variable extent with the Golgi marker (Fig. 5d). Even apparently peripheral elements in which apical/basolateral cargo was partially segregated were also positive for gp27 (Fig. 5d, inserts) suggesting that these were Golgi elements. Although peripheral Golgi/TGN structures in a given focal plane may appear as distinct entities 3D stacks indicate they are connected by thin tubules (see Supplementary Information movie to Fig. 5A). Together, these results suggest that segregation most probably occurs in the TGN.

Apical and basolateral cargo move to the periphery in separate TCs. Apical and basolateral TCs were tracked to determine whether on exit from the Golgi they remained distinct until arrival at the plasma membrane. Figure 6a shows a frame of a movie (see Supplementary Information movie) taken 23 min after release from the 19.5 °C block. Transport containers contained either apical or basolateral cargo, rarely both.

A running subtraction of the frames cancels out stationary structures to reveal only moving elements. A projection of the subtracted images shows the tracks followed by TCs (Fig. 6b). TCs remained separate until the cell periphery, indicated by tracks exclusive for a single type of cargo (Fig. 6b). Tracks were rarely labelled by both cargo. These results indicate that the segregation of apical and basolateral cargo is maintained to the plasma membrane.

Basolateral post-Golgi TCs do not intersect with endocytic structures. It has been proposed that certain basolateral cargo traverse endosomes *en route* from the Golgi to the plasma membrane[29,31]. Our earlier results indicated that post-Golgi TCs did not colocalize with endosomes in fixed cells[22], but it remained possible that they transiently traversed endocytic structures before reaching the surface. To test this, we labelled endocytic structures with Texas-Red-transferrin or -dextran for 3 h in PtK_2 cells expressing our basolateral marker and imaged the cells, starting 20 min after release of exocytic cargo from the ER. Figure 7a and c show the distribution of VSVG3–SP–YFP and Texas-Red-transferrin or -dextran, respectively. Because of the high density of late endocytic

© 2001 Macmillan Magazines Ltd

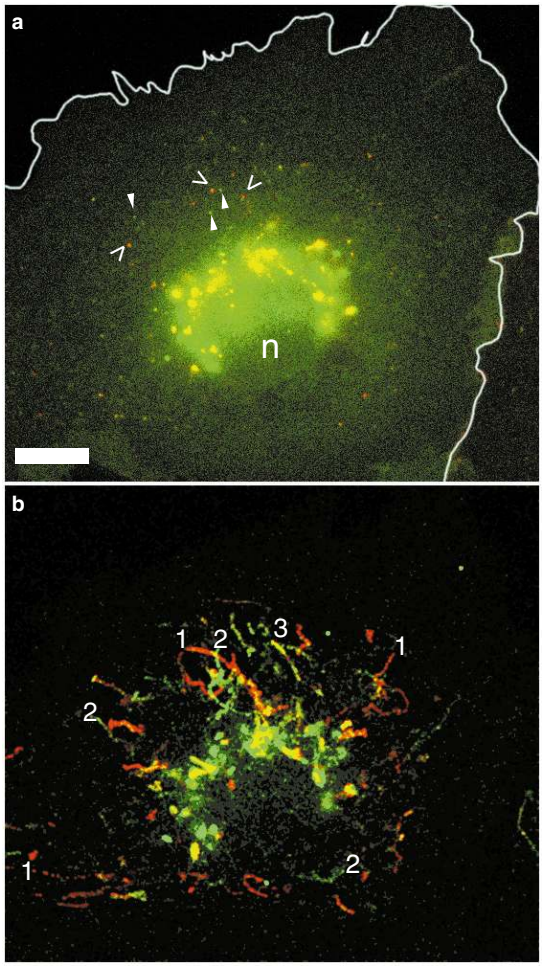

Figure 6 **Apical and basolateral cargo move in separate TCs to the cell periphery.** See also Supplementary Information. PtK_2 cells were infected with adenoviruses expressing VSVG3–SP–YFP (red) and CFP–GL–GPI (green). **a**, A movie frame taken 23 min after release from the 19.5 °C block. Individual TCs in the cell periphery containing VSVG3–SP–YFP or CFP–GL–GPI are indicated (> and arrowheads, respectively). Images are adjusted so that weak structures in the cell periphery are visible (the Golgi is saturated). **b**, Two-frame running subtraction of successive frames shows only the moving structures. Moving TCs containing basolateral cargo (1), apical cargo (2), or both cargo (3) are indicated by numbers at the end of the track. The nucleus (n) and cell boundary (white line) are indicated. Scale bar, 10 μm.

structures in the perinuclear region, there was some incidental overlap near the Golgi; however, in the cell periphery overlap was not significant, and exocytic and endocytic structures moved independently (Fig. 7; and Supplementary Information movies).

To ensure that we did not miss transient trafficking of VSVG3–SP–YFP into endosomes, we manually tracked the movement of exocytic and endocytic cargo (Table 1). Most TCs were positive for either cargo, and rarely contained both; those that did were primarily static. Out of 133 TCs containing exocytic cargo, only 1 moving TC contained endocytic cargo. These observations indicate that most of VSVG3–SP–FP does not traverse endosomes on its way to the cell surface.

Total internal reflection microscopy reveals exocytic 'hot spots' in the plasma membrane and size differences between apical and basolateral carriers. Basolateral cargo was often found in larger and more fluorescent TCs as compared with apical cargo (for example, see Fig. 4). Because of background fluorescence, these intensity differences were difficult to quantitate by standard wide-field microscopy. To address further the size distribution of apical and basolateral TCs, we used TIR microscopy[31]. In this approach only fluorophores near the bottom of the cell are excited (~50 nm penetration depth in our set-up). TIR provides excellent signal-to-noise that allowed us and others to detect fusion of TCs with the plasma membrane[23,32]. While previously we examined only VSVG3–SP–YFP, we now have also included an apical marker. In addition, we implemented a semi-automated software tool for detection, quantitation and plotting of fusion events. This allowed us to analyse many more fusion events than previously possible and consequently lead to some unexpected observations.

In our TIR microscopy movies (Supplementary Information), TCs became exponentially brighter as they approached the cell surface. Fusion resulted in a bright 'flash' as fluorescent cargo was inserted into the plasma membrane; the intensity of the flash was related to the amount of fluorophore released into the membrane. Direct visual inspection of the movies yielded no obvious pattern for fusion of either marker, with the exception that sometimes fusion was excluded from regions of the cell periphery — consistent with our previous observations[23]. This could not be trivially explained by poor contact, for it could clearly be observed in regions where the plasma membrane was in close apposition with the coverslip (Fig. 8a, asterisk). When we plotted the coordinates of hundreds of fusion events, specific plasma-membrane 'hot spots' for exocytosis were apparent for both types of carriers (Fig. 8a and c, yellow arrowheads). Often 5 – 10 events were detected in micron-sized 'hot spots', with over 30 events in particularly active sites; however, an important consideration is that even randomly distributed events will occasionally show clusters or patterns.

To assess our data critically, we randomly generated by computer an equal number of artificial fusion events within the cell boundary (Fig. 8b and d). Clustering here was only occasionally observed (orange arrowheads). To quantitate differences between our data and the Monte Carlo simulations, we performed a nearest-neighbour analysis (see Methods; Fig. 8g and h). The actual data sets for both cargo differed significantly from the upper and lower envelopes of the simulations. Numerically, our observed data for apical and basolateral fusions were 19- and 10-fold larger than the maximal values of the simulations, respectively. Thus, these data show that the last event in constitutive exocytosis is non-random and can occur at specific sites.

To address putative differences in the size of the TCs, we calculated the difference in fluorescence between the docked and fused state (Fig. 8e and f). For both apical and basolateral markers most TCs gave a relatively weak fusion signal, suggesting that most TCs were relatively small. In contrast, more intense fusion events, highlighted by green bars in Fig. 8e and f, were strikingly different. Although only 1.6% of apical TCs were present in this region and accounted for 6.9% of the total fluorescence, 6.2% of the basolateral TCs in the same region accounted for 23.8% of the total fluorescence.

Discussion

Several technical advances have allowed us to observe directly the sorting and trafficking of apical and basolateral cargo in living cells with minimal perturbation. First, the adenovirus expression system allows efficient co-expression of markers without shutting down host-cell protein synthesis. Second, spectral variants of GFP allow two proteins to be visualized concurrently. Third, TIR allowed us to study fusion at the plasma membrane. Last, using time-lapse digital microscopy, we were able to compare the dynamics of two proteins with high temporal resolution: simple and direct experiments to observe the cellular mechanisms of post-Golgi sorting and trafficking.

We initiated these studies in polarized MDCK cells; however, to view sorting and trafficking adequately, this would require fast 2-colour 4D (3D over time) confocal-like imaging, which is currently unfeasible. We therefore switched to non-polarized PtK_2 cells, which are much better suited for video microscopy because they are flatter.

© 2001 Macmillan Magazines Ltd

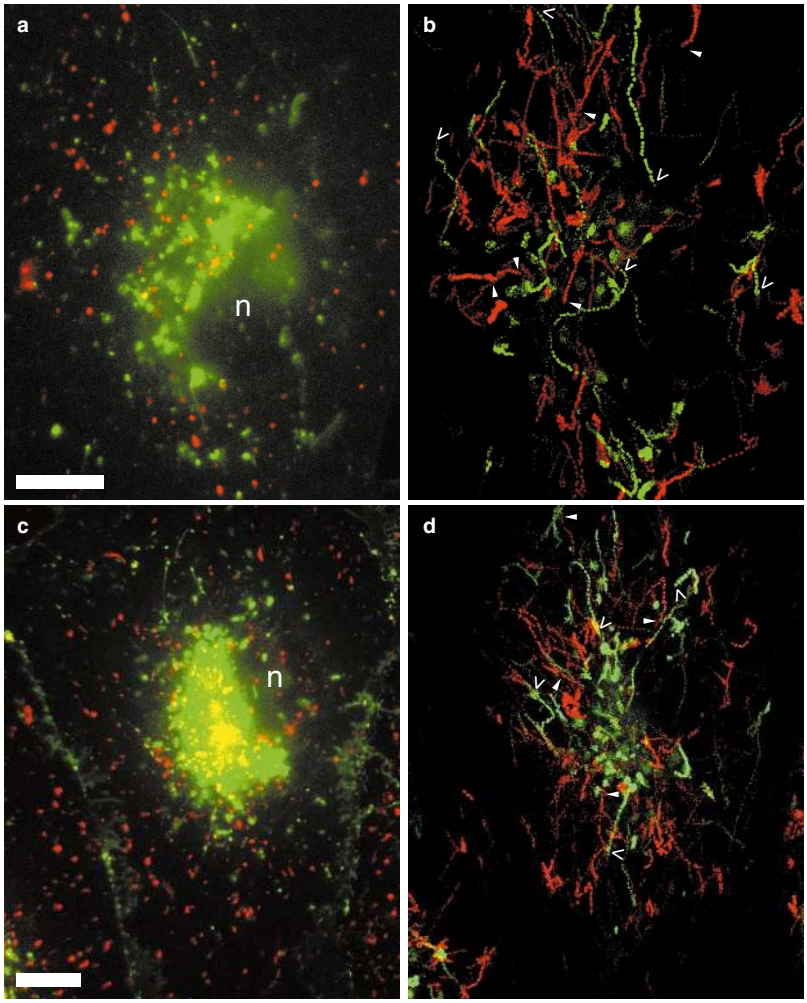

Figure 7 **Basolateral post-Golgi TCs do not intersect with endocytic structures.** See also Supplementary Information. PtK_2 cells were infected with an adenovirus expressing VSVG3–SP–YFP (green). The endocytic pathway (red) was loaded for 3 h with Texas-Red-transferrin (**a, b**) or Texas-Red-dextran (**c, d**). **a**, **c**, Single images from movies acquired 20 min after VSVG3–SP–YFP had been released from the ER. **b**, **d**, Two-frame running subtraction of successive frames shows only the moving structures. Moving TCs containing basolateral (>) and endocytic cargo (arrowheads) are indicated by the respective symbols at the end of the track. The nucleus (n) is indicated. Scale bars, 10 μm.

To characterize our system and help address the site of apical/basolateral sorting, we observed trafficking of cargo in cells expressing FP-labelled Golgi or TGN resident proteins. When VSVG3–SP–FP was released from the ER as a pulse, the cargo entered the Golgi stack and initially overlapped with the T2–FP Golgi marker, but then progressively polarized. The corollary experiment with a labelled TGN marker showed that the cargo initially segregated from the TGN, and then overlapped. Together with the separation of TGN and Golgi elements, these studies confirmed that the pulse of cargo progressed from the Golgi stack to the TGN before exit. Basolateral cargo segregated into large domains separate from Golgi resident proteins with dynamics that were highly similar to those of separation from apical cargo. Large, continuous regions of VSVG3–SP–FP pulled away from a stable element to form a segregated domain from which various sized TCs subsequently exited. Together with our data on FP–GL–GPI and VSVG3–SP–FP sorting, this suggests that apical/basolateral segregation occurs in the TGN. Additional evidence supporting segregation in the TGN was obtained by triple-colour immunofluorescence with a Golgi marker and both types of cargo.

Separate cargo domains formed rapidly and were large enough—on the order of microns—to be easily visualized in living cells. After only 10 min of release from a Golgi block, large regions were observed to contain mainly one type of cargo. The dynamics of their formation suggests that they were formed by lateral segregation within the membrane of the TGN: large micron-sized regions of one type of cargo segregated rapidly from a stable TGN element containing both apical and basolateral cargo. Cargo domains showed complementary dynamics over time, indicating that they were different regions of the same physical element. This suggests a model in which the primary sorting event occurs by lateral segregation.

One mechanism of organizing cargo into domains is that of clustering. Apical and basolateral domain formation on Golgi elements is reminiscent of cell-surface antibody-induced clustering of proteins and lipids into separate domains[33]. By analogy, apical and basolateral cargo in the TGN may similarly segregate: apical, GPI-linked cargo partitions preferentially to rafts, whereas basolateral cargo partitions preferentially away from rafts. The finding that apical delivery of GPI-anchored proteins requires not only raft association, but also *N*-glycosylation[34] suggests that clustering of apical cargo might be mediated by a lectin that recognizes *N*-glycans, although

© 2001 Macmillan Magazines Ltd

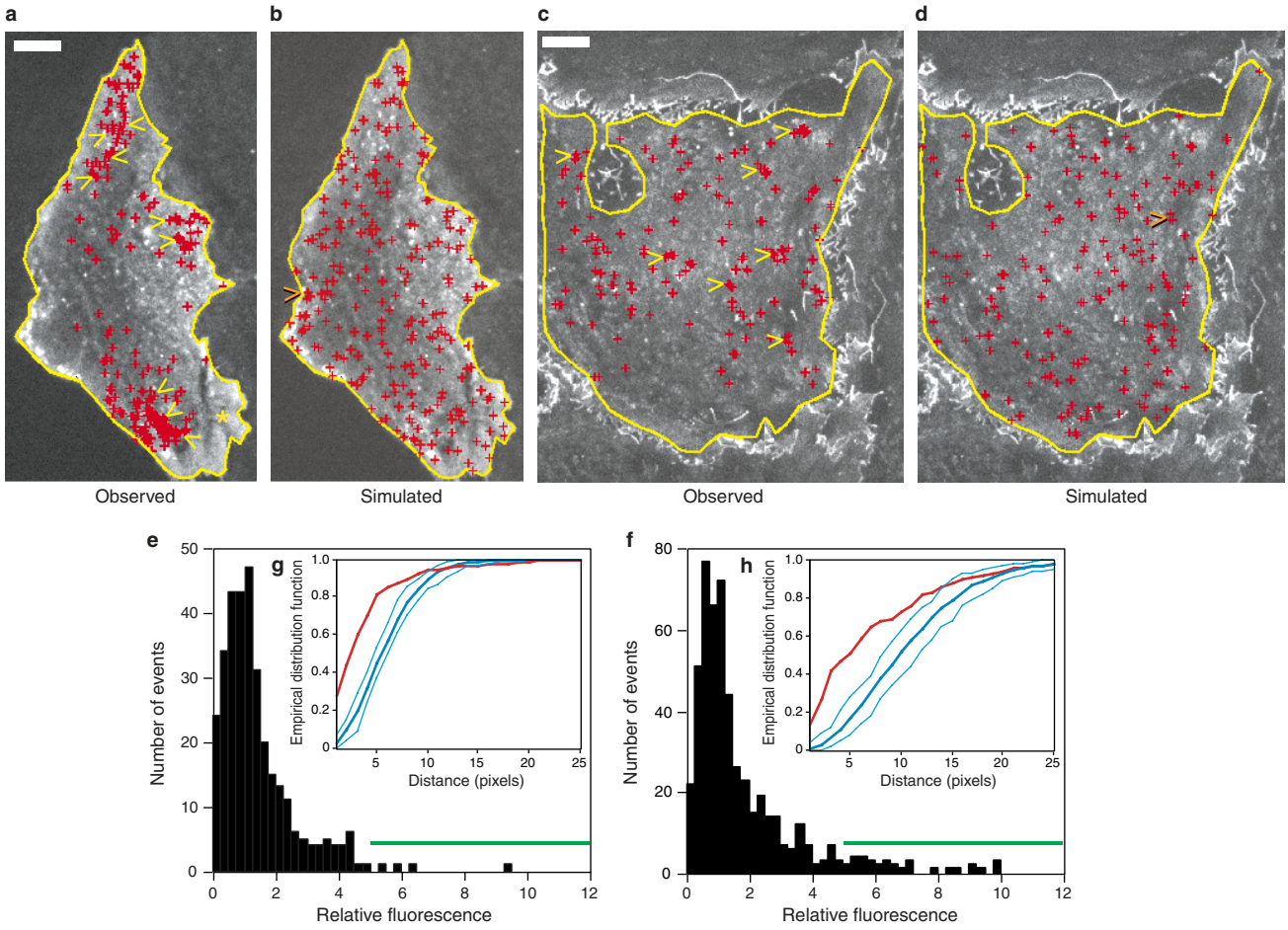

Figure 8 **Fusion of apical and basolateral TCs at plasma membrane 'hot spots'.** See also Supplementary Information. PtK_2 cells were infected with adenoviruses expressing YFP–GL–GPI (**a**, **b**, **e**, **g**) or VSVG3–SP–YFP (**c**, **d, f, h**) and fusion of cargo at the plasma membrane was monitored by TIR microscopy at 2 Hz. Apical and basolateral samples were treated identically and no ER block was used. **a**, **c**, All fusion events observed for YFP–GL–GPI (1,400 frames, 231 events; **a**) and VSVG3–SP–YFP (1,000 frames, 171 events; **c**) are marked by red crosses. Hot spots (>) where many fusion events occurred are indicated. **b**, **d**, The same number of fusion events randomly positioned in the cell by computer. **g**, **h**, Empirical distribution function plots of nearest-neighbour distances (see Methods) for the observed fusion events (red) and the mean (thick blue line) from the random simulations (99) generated for YFP–GL–GPI (**g**) and VSVG3–SP–YFP (**h**). Upper and lower simulation envelopes are drawn as thin blue lines. The curves obtained for the experimentally observed fusion events clearly showed an excess of small nearest-neighbour distances, characteristic of clustered patterns. This indicates that fusion at the plasma membrane is not random. **e**, **f**, Histograms of the relative fluorescence intensity for all fusion events observed in **a** and **c**, respectively. (See Results for explanation of the green bar.) Scale bars, 10 μm.

an apical-sorting lectin remains to be identified[35]. A clathrin adaptor present in MDCK cells, the μ1B subunit of AP-1, recognizes basolateral sorting information in the cytosolic tail of a subset of cargo to mediate basolateral targeting[13]. The Golgi localization of AP-4 suggests that this adaptor might bind to different cytoplasmic signals on another subset of cargo proteins[36]. The possibility that large domains on the TGN could be organized by different coat proteins and adaptors is consistent with electron microscopy observations of TGN regions containing distinct coats[36,37].

Analysing the arrival of TCs at the cell surface by TIR microscopy indicates distinct morphological differences between apical and basolateral carriers. Although almost all apical cargo is delivered in small TCs, ~25% of basolateral cargo is delivered in larger TCs. The observation that most of the TCs fusing at the cell surface are small raises the issue of how these TCs are formed in the TGN. Obviously the mechanisms by which they are generated in the TGN and how they are modulated during transport remain to be explored. In our current working model of apical/basolateral sorting events occur as follows: (1) signal recognition; (2) clustering, which induces (3) lateral organization of discrete domains in the TGN; and (4) TC generation and exit, with distinct TCs arising from distinct exit domains.

Transport containers that contain only one type of cargo remained separate until they appeared to fuse with the plasma membrane (Fig. 6 Supplementary Information movie, red circle). Additional studies with combined epifluorescence and TIR microscopy indicate that the fluorescent 'puff' observed here most probably represents a fusion event[23]. We occasionally observed fusing TCs that contained both types of cargo (Fig. 6 Supplementary Information movie, yellow circle). Further sorting or separation of cargo within a moving TC was not observed, suggesting that if a TC left the TGN with both types of cargo it maintained this composition until it fused. Sorting is therefore not completely efficient, and delivery of such mixed TCs might account for the mis-sorting observed in polarized cells.

It has been suggested that endosomes may be the final sorting station for basolateral cargo[29,30]. On the other hand, an immunoelectron microscopy study showed little overlap of newly synthesized VSVG and the endosomal marker transferrin[39]. But it is possible that

© 2001 Macmillan Magazines Ltd

if sorting in endosomes was rapid, then a transient overlap may have been missed. Here, we have directly observed in live cells that most basolateral cargo traffics independently of endocytic structures. Because we can observe a synchronous pulse of cargo, and rapidly acquire dual images, it is unlikely that we failed to observe transient delivery of a significant portion of basolateral cargo to endosomes. It is conceivable that trafficking through endosomes might be different for other types of basolateral proteins. It is also possible that exocytic sorting by endosomes may be different in polarized MDCK cells which express specific AP-1 adaptor complexes[12]. Nevertheless, most of VSVG3–SP–FP was delivered independently of endocytic structures. Thus, endosome-based sorting is not *per se* a prerequisite for delivery to the plasma membrane.

Our direct dual-colour visualization of sorting and trafficking of apical and basolateral cargo in non-polarized cells confirms biochemical evidence that non-polarized cells possess cognate apical and basolateral transport pathways[8–10]. Sorting in the TGN therefore generates different classes of TCs that, by targeting to different physical regions, can generate overall cellular polarity. Cargo delivery must be coordinated with other determinants of cell polarity, such as cell adhesion[40] and cytoskeletal rearrangements. In this regard, it is interesting that our TIR microscopy studies revealed plasma membrane 'hot spots' for constitutive exocytosis of both classes of carriers. We stress that we could only observe fusion readily with this sensitive high *z* resolution TIR set-up. Moreover, fusion at these hot spots was often spaced apart by 30 s or longer and so was not apparent by eye. The restricted exocytic sites were only evident when hundreds of events were tracked and plotted. Efforts are underway to elucidate the mechanism(s) responsible for such specialized delivery — preliminary results implicate microtubules. These hot spots were observed in stationary non-polarized cells, which suggests that a mechanism for restricted delivery may already be in place in many cell types. Moreover, it will be curious to see if and how redistribution of specialized exocytic sites occurs during cellular polarization.

Note added in proof: The use of multicolour imaging is described in Rustom *et al.* (Analysis of fast dynamic processes in living cells: high-resolution and high-speed dual-color imaging combined with automated image analysis. *Biotechniques* **28,** 722–730; 2000). □

Methods

Cell culture.

PtK_2 and MDCK II cells were grown in MEM, 100 U ml^{-1} penicillin, 100 μg ml^{-1} streptomycin, 2 mM L-glutamine, 1 × non-essential amino acids, and 10% fetal calf serum (complete medium). Cells were grown on 11-mm coverslips in complete medium without phenol-red for epifluorescence or on 1-mm thick, 30-mm diameter sapphire slides (Rudolf Brügger AG, Minusio, Switzerland) for TIR microscopy.

Constructs and generation of recombinant adenoviruses.

FP–GL–GPI is a GPI-anchored protein containing the signal sequence of lactase-phlorizin hydrolase LPH[41], FP, and a consensus *N*-glycosylation site fused to the GPI-attachment signal of lymphocyte-function-associated antigen 3 (LFA-3; ref. 42). The sequence encoding the GPI-attachment signal was released from Fc_RI-GPI[43] as a *Hin*dIII/*Not*I fragment, and transferred into pEGFP–N1 (Clontech), yielding plasmid pN1–FcRGPI. A DNA fragment encoding the signal sequence was generated by PCR with a *Nhe*I site at the 5' end, and a *Pst*I site at the 3' end. Primers used were 5'-TAGCTAGCCAC-CATGGAGCTCTTTTGG-3' and 5'-ATCCTGCAGAGATTCCCAGTCTGA-3'. This PCR fragment was ligated into pEGFP-N1 yielding the secretory protein LGFP. Using PCR, we modified LGFP with a *Hin*dIII site at the 5' end, and a *Bam*HI-compatible in-frame *Bcl*I site at the 3' end. We used the primers 5'-CCAAGCTTAGCTAGCCACCATGGAGC-3' and 5'-GCTGATCATACTGGTGCTGTCCG-GAGCCGTTTCCTCCATACTTGTACAGCTCGTCC-3' (the added *N*-glycosylation site is underlined). The product was inserted into *Hin*dIII/*Bam*HI digested pN1–FcRGPI to generate GFP–GL–GPI. C/YFP versions were constructed by swapping FP coding regions as *Age*I/*Bsr*GI fragments. Adenoviruses were generated as described[44]. FP–GL–GPI was released as a *Bgl*II/*Not*I fragment that was ligated into pShuttle–CMV.

VSVG3–SP–FP is based on VSVG3–FP[21]; it differs by having a longer spacer between VSVG and FP (DLPAEQKLISEEDLDPPVAT compared with DPPVAT), which was made using two complementary oligonucleotides creating *Bam*HI sites at both ends (5'-GATCTCCCCGCCGAACAGAAACTCATCTC-CGAAGAAGACCTG-3', and 5'-GATCCAGGTCTTCTTCGGAGATGAGTTTCTGTTCGGCGGGGA-3'). The annealed oligonucleotides were ligated directionally into *Bam*HI digested VSVG3–GFP, yielding VSVG3–SP–GFP. C/YFP versions were obtained by swapping FP coding regions as *Bam*HI/*Not*I fragments. Adenoviruses were generated as described above.

TGN38–Y/CFP were constructed from ΔpMEP4–TGN38–EGFP[27]. Briefly, the TGN38 portion of TGN38–EGFP was released from ΔpMEP4–TGN38–EGFP as a *Kpn*I/*Bse*RI fragment that was used for a triple ligation with the 3,990-bp *Kpn*I/*Bsr*GI and 694-bp *Bse*RI/*Bsr*GI fragments of pEY/CFP–N1.

Transient transfection and generation of stable cell lines.

Transient transfection using calcium phosphate precipitation and generation of stable PtK_2 cell lines was done as described[22]. The behaviour of transiently and stably expressing cells was indistinguishable.

Adenovirus infection.

MDCK cells were grown on 12-mm, 0.4-μm pore Transwell polycarbonate filters (Costar). Seventy-six hours after seeding, cells were infected from the apical side for 1 h at 37 °C with adenoviruses in 75 μl of complete medium. MDCK and PtK_2 cells grown on coverslips in 3-cm dishes were infected identically in 500 μl of medium. After changing medium, cells were incubated for 6–20 h at 37 °C or 39.5 °C, and then used for biochemical assays or microscopy.

Triton X-100 extraction, endoH digestion and PIPLC treatment.

Infected MDCK cells were labelled for 10 min with 83 μCi of [^{35}S]methionine (Amersham) and, after a chase for 90 min, cells were extracted on ice for 30 min with 300 μl of 1% (wt/vol) Triton X-100 in 50 mM Tris-HCl pH 7.4, 150 mM NaCl, 2 mM EDTA, 2 mM dithiothreitol. After centrifugation for 30 min at 120,000*g*, FP fusion proteins were immunoisolated from Triton X-100-soluble and -insoluble fractions. After separation on 10% polyacrylamide gels[45], individual bands were quantitated using a Fuji BAS image plate reader and AIDA v2.0 software (Raytest Isotopenmessgeräte, Straubenhardt, Germany). For endoglycosidase H digestion or phosphatidylinositol phospholipase C (PIPLC) treatment, MDCK cells were labelled for 8 min and chased for 60 min. They were lysed in 120 μl of lysis buffer (2% NP-40, 0.2% SDS in PBS), and FP fusion proteins were immunoisolated. Aliquots of the immunoprecipitates were treated with endoH according to the manufacturer (Roche Diagnostics) and analysed on 10% gels. Other aliquots were taken up in 25 mM Tris-HCl pH 7.5, 0.5 mM $CaCl_2$, and incubated overnight at 37 °C in the presence of 50 units of PIPLC (Oxford GlycoSciences, Abingdon, UK).

Surface distribution in MDCK cells.

MDCK cells were double infected with adenoviruses expressing FP–GL–GPI and VSVG3–SP–FP. After an incubation for 18 h at 37 °C, they were labelled for 15 min with 83 μCi of [^{35}S]methionine, and chased for 90 min at 37 °C. Filters were biotinylated from either the apical or basolateral side for 20 min on ice with 1 mg ml^{-1} sulfo-NHS-LC-biotin (Pierce) in PBS. After quenching of non-reacted sulfo-NHS-LC-biotin, cells were lysed in 300 μl of lysis buffer, and FP fusion proteins were immunoprecipitated. They were released from protein A/Sepharose CL4B (Amersham) by boiling for 5 min in 20 μl of 10% SDS. After addition of 200 μl of lysis buffer, aliquots of 30 μl (total fraction) and 170 μl (surface fraction) were made, and biotinylated FP fusion proteins were precipitated from the surface fraction using immobilized streptavidin (Roche Diagnostics). After separation on 10% gels, individual bands were quantitated, and apical/basolateral distribution was calculated from filter pairs.

Labelling of endocytic organelles.

PtK_2 cells infected with VSVG3–SP–YFP adenoviruses were incubated for 12 h at 39.5 °C. After addition of Texas-Red-dextran (0.5 mg ml^{-1}) or Texas-Red-transferrin (0.25 mg ml^{-1}) (Molecular Probes) for 3 h in complete dye-free medium, VSVG3–SP–YFP was released from the ER by lowering the temperature to 32 °C for 15–40 min. Cells were washed once in dye-free medium and used immediately for microscopy.

Immunofluorescence.

PtK_2 cells infected with YFP–GL–GPI and VSVG3–SP–CFP adenoviruses were incubated for 2 h at 19.5 °C, and were fixed after a shift to 37 °C for 10 min. We carried out immunolabelling of saponin-permeabilized cells as described[27] using Alexa546 goat anti-rabbit secondary antibodies (Molecular Probes).

Confocal, TIR and epifluorescence microscopy.

Images of fixed MDCK cells were acquired on a Zeiss LSM 510 confocal microscope with a 63× oil planapochromat lens (NA 1.4; Carl Zeiss). We excited YFP with the 488-nm line of an argon laser. Excitation and emission was monitored using a 505-nm longpass filter. To image living cells, we mounted coverslips in an aluminium chamber containing phenol-red-free CO_2-independent medium (GibcoBRL), 5% fetal calf serum, and 20 μg ml^{-1} cycloheximide. Confocal images of living PtK_2 cells were acquired using line-interlaced sequential excitation on the Compact Confocal Camera as described[46]. CFP was excited with a 430-nm laser line (Directly Doubled Diode/D3, Coherent) and imaged through a NT80/20/543 beamsplitter and 440–505-nm bandpass and 525-nm longpass emission filters. YFP was excited with the 514-nm laser line and imaged through a 525-nm longpass emission filter.

Total internal reflection microscopy was carried out after a 19.5 °C block at 37 °C as described[23]. Time-lapse epifluorescence video microscopy was performed using an Olympus IX70 (Olympus, Hamburg, Germany) inverted microscope equipped with a polychrome II monochromator (TILL Photonics, Martinsried, Germany), a custom filter block for simultaneous visualization of YFP and CFP (AHF Analysentechnik, Tübingen, Germany), a 100× oil-immersion lens (NA 1.35, Olympus) attached to a PIFOC z-SCAN (Physik Instrumente, Waldbronn, Germany), an incubation chamber (37 °C), and a 12-bit CCD digital camera IMAGO (0.134 μm $pixel^{-1}$; 2 × 2 binning) (TILL Photonics), controlled by TILLvisION v3.3 software (TILL Photonics). Switching of excitation wavelengths (430 nm and 500 nm for CFP and YFP, respectively) took about 2 ms, and data acquisition times typically ranged from 50 to 500 ms per image. Three dimensional reconstruction of MDCK cells acquired on a Leica microscope was done using OpenLab software (Improvision, Coventry, UK).

Data processing.

Sequences of YFP and CFP images from the video microscope were merged as RGBs using TILLvisION v3.3. They were exported as single TIFF files, and further processed using Adobe Photoshop 5.0 and Illustrator 7.0, or they were converted into QuickTime movies using IPLab v.3.2 (Scanalytics, Fairfax, VA). Brightest point projections of *z* stacks, and analysis of moving structures were done using TILLvisION v3.3 macros. Colocalization analysis of exocytic and endocytic cargo was done manually by tracking single- and double-positive structures in the acquired time sequences. Representative intensity profiles through the Golgi were obtained with the line profile tool of TILLvisION v3.3. Line profiles were linearly scaled after background subtraction to maximize overlap of apical and basolateral cargo. Scale factors for the red channel were respectively 1.3, 1.6 and 1.7 in Fig. 3d–f. Additional colocalization analysis of apical and basolateral cargo was done on brightest point projections through the Golgi

© 2001 Macmillan Magazines Ltd

using TILLvisION v3.3 macros. Anonymous data sets were randomly selected based on the YFP signal and given a threshold, such that overlap of different cargo was maximized in the Golgi. As thresholding is nonlinear and may cause under- or overestimation of colocalization, all analysis was performed in a blind manner. Colocalization analysis of the binarized images was applied to calculate the total area and intensity of thresholded objects. To measure export kinetics, cells were imaged at 1 frame min^{-1} after release from the Golgi block. Cargo fluorescence in the Golgi and over the total cell area were determined using the kinetic selection tool of TILLvisION v3.3. Export of cargo was displayed as the ratio of Golgi relative to cell-surface fluorescence, calculated as Golgi fluorescence/(Total fluorescence – Golgi fluorescence).

Analysis of fusion events at the plasma membrane.

To analyse TIR fusion events, we implemented a custom semi-automated tracking and analysis software tool using Matlab v5.1 (MathWorks, Natick, MA)[23]. Briefly, the user selected points associated with fusion events for each frame of the sequence. Total fluorescence around these points was calculated for previous frames, and the difference between docked and fused states was calculated. To describe the nature of the spatial distribution of these events, we have used a stochastic model for spatial randomness, which asserts that any location has equal probability of receiving an event and that points are independent from one another. To test this model against our data, we have used a Monte Carlo test that can be described as follows: u_{obs} represents the observed value of a statistic U; u_i (i=2,...,s) correspond to values generated by 99 independent simulations (s=100) under the hypothesis of randomness. The probability of finding u_{obs} larger than the set of random values u_i (i=2,...,s) is 1/s. Thus, we have a confidence level of 99%. To obtain information about the spatial distribution of observed and random data, we measured the distance between neighbouring events (that is, nearest-neighbour analysis). For n fusion events, d_i denotes the distance from the ith event to the nearest other event. The empirical distribution function under spatial randomness[46], $\hat{G}_{obs}(d)$, of the nearest-neighbour distances is

$$\hat{G}_{\mathrm{obs}}(d) = \frac{\#\,(d_i \le d)}{n},$$

where # represents 'the number of'. As events are located independently within a region $|A|$, the theoretical distribution[47] can be approximated by

$$G(d) = 1 - (1 - \frac{\Pi d^2}{|A|})^{(n-1)}$$

The empirical distribution function $\hat{G}_i(d)$ was calculated for i=2,...,100. A measure of discrepancy between the simulations $_i(d)$ and the theoretical distribution $G(d)$ over a range of distances, d, is

$$u_i = \int \{\hat{G}_i(r) - G(r)\}^2\, dr.$$

This represents the area under $\hat{G}_i(d)$ and $G(d)$. If the value $u_{obs} > u_i$ (i=2,...,100), then the distribution of fusion events is non-random. This can also be displayed graphically as a plot of $G_{obs}(d)$ (see Fig. 8). If the data are non-random, $G_{obs}(d)$ will be outside the simulation envelopes.

RECEIVED 22 JUNE 2000; REVISED 29 AUGUST 2000; ACCEPTED 5 OCTOBER 2000; PUBLISHED 15 JANUARY 2001.

1. Ikonen, E. & Simons, K. Protein and lipid sorting from the trans-Golgi network to the plasma membrane in polarized cells. *Semin. Cell Dev. Biol.* **9,** 503–509 (1998).
2. Yeaman, C., Grindstaff, K. K. & Nelson, W. J. New perspectives on mechanisms involved in generating epithelial cell polarity. *Physiol. Rev.* **79,** 73–98 (1999).
3. Simons, K. *et al.* Biogenesis of cell-surface polarity in epithelial cells and neurons. *Cold Spring Harb. Symp. Quant. Biol.* **57,** 611–619 (1992).
4. Winckler, B., Forscher, P. & Mellman, I. A diffusion barrier maintains distribution of membrane proteins in polarized neurons. *Nature* **397,** 698–701 (1999).
5. Bretscher, M. S. Moving membrane up to the front of migrating cells. *Cell* **85,** 465–467 (1996).
6. Traub, L. M. & Kornfeld, S. The trans-Golgi network: a late secretory sorting station. *Curr. Opin. Cell Biol.* **9,** 527–533 (1997).
7. Mostov, K. E. & Cardone, M. H. Regulation of protein traffic in polarized epithelial cells. *BioEssays* **17,** 129–138 (1995).
8. Müsch, A., Xu, H., Shields, D. & Rodriguez-Boulan, E. Transport of vesicular stomatitis virus to the cell surface is signal mediated in polarized and nonpolarized cells. *J. Cell Biol.* **133,** 543–558 (1996).
9. Yoshimori, T., Keller, P., Roth, M. G. & Simons, K. Different biosynthetic transport routes to the plasma membrane in BHK and CHO cells. *J. Cell Biol.* **133,** 247–256 (1996).
10. Keller, P. & Simons, K. Post-Golgi biosynthetic trafficking. *J. Cell Sci.* **110,** 3001–3009 (1997).
11. Mellman, I. *et al.* Molecular sorting in polarized and non-polarized cells: common problems, common solutions. *J. Cell Sci.* **17** (Suppl.), 1–7 (1993).
12. Matter, K. & Mellman, I. Mechanisms of cell polarity: sorting and transport in epithelial cells. *Curr. Opin. Cell Biol.* **6,** 545–554 (1994).
13. Fölsch, H., Ohno, H., Bonifacino, J. S. & Mellman, I. A novel clathrin adaptor complex mediates basolateral targeting in polarized epithelial cells. *Cell* **99,** 189–198 (1999).
14. Scheiffele, P. & Simons, K. in *Epithelial Morphogenesis in Development and Disease* (eds Birchmeier, W. & Birchmeier, C.) 41–71 (Harwood Academic, Newark, New Jersey, 1999).
15. Rodriguez-Boulan, E. & Gonzalez, A. Glycans in post-Golgi apical targeting: sorting signals or structural props? *Trends Cell. Biol.* **9,** 291–294 (1999).
16. Simons, K. & Ikonen, E. Functional rafts in cell membranes. *Nature* **387,** 569–572 (1997).
17. Rindler, M. J., Ivanov, I. E., Plesken, H., Rodriguez-Boulan, E. & Sabatini, D. D. Viral glycoproteins destined for apical or basolateral plasma membrane domains traverse the same Golgi apparatus during their intracellular transport in doubly infected Madin–Darby canine kidney cells. *J. Cell Biol.* **98,** 1304–1319 (1984).
18. Fuller, S. D., Bravo, R. & Simons, K. An enzymatic assay reveals that proteins destined for the apical or basolateral domains of an epithelial cell line share the same late Golgi compartments. *EMBO J.* **4,** 297–307 (1985).
19. Griffiths, G. & Simons, K. The trans Golgi network: sorting at the exit site of the Golgi complex. *Science* **234,** 438–443 (1986).
20. Hirschberg, K. *et al.* Kinetic analysis of secretory protein traffic and characterization of Golgi to plasma membrane transport intermediates in living cells. *J. Cell Biol.* **143,** 1485–1503 (1998).
21. Nakata, T., Terada, S. & Hirokawa, N. Visualization of the dynamics of synaptic vesicle and plasma membrane proteins in living axons. *J. Cell Biol.* **140,** 659–674 (1998).
22. Toomre, D., Keller, P., White, J., Olivo, J. C. & Simons, K. Dual-color visualization of trans-Golgi network to plasma membrane traffic along microtubules in living cells. *J. Cell Sci.* **112,** 21–33 (1999).
23. Toomre, D., Steyer, J. A., Keller, P., Almers, W. & Simons, K. Fusion of constitutive membrane traffic with the cell surface observed by evanescent wave microscopy. *J. Cell Biol.* **149,** 33–40 (2000).
24. Miyawaki, A. *et al.* Fluorescent indicators for Ca^{2+} based on green fluorescent proteins and calmodulin. *Nature* **388,** 882–887 (1997).
25. Röttger, S. *et al.* Localization of three human polypeptide GalNAc-transferases in HeLa cells suggests initiation of *O*-linked glycosylation throughout the Golgi apparatus. *J. Cell Sci.* **111,** 45–60 (1998).
26. Storrie, B. *et al.* Recycling of Golgi-resident glycosyltransferases through the ER reveals a novel pathway and provides an explanation for nocodazole-induced Golgi scattering. *J. Cell Biol.* **143,** 1505–1521 (1998).
27. Girotti, M. & Banting, G. TGN38-green fluorescent protein hybrid proteins expressed in stably transfected eukaryotic cells provide a tool for the real-time, *in vivo* study of membrane traffic pathways and suggest a possible role for ratTGN38. *J. Cell Sci.* **109,** 2915–2926 (1996).
28. Füllekrug, J. *et al.* Localization and recycling of gp27 (hp24γ3): Complex formation with other p24 family members. *Mol. Biol. Cell* **10,** 1939–1955 (1999).
29. Leitinger, B., Hille-Rehfeld, A. & Spiess, M. Biosynthetic transport of the asialoglycoprotein receptor H1 to the cell surface occurs via endosomes. *Proc. Natl Acad. Sci. USA* **92,** 10109–10113 (1995).
30. Futter, C. E., Connolly, C. N., Cutler, D. F. & Hopkins, C. R. Newly synthesized transferrin receptors can be detected in the endosome before they appear on the cell surface. *J. Biol. Chem.* **270,** 10999–11003 (1995).
31. Axelrod, D. Cell–substrate contacts illuminated by total internal reflection fluorescence. *J. Cell Biol.* **89,** 141–145 (1981).
32. Schmoranzer, J., Goulian, M., Axelrod, D. & Simon, S. M. Imaging constitutive exocytosis with total internal reflection fluorescence microscopy. *J. Cell Biol.* **149,** 23–31 (2000).
33. Harder, T., Scheiffele, P., Verkade, P. & Simons, K. Lipid domain structure of the plasma membrane revealed by patching of membrane components. *J. Cell Biol.* **141,** 929–942 (1998).
34. Benting, J. H., Rietveld, A. G. & Simons, K. *N*-Glycans mediate the apical sorting of a GPI-anchored, raft-associated protein in Madin–Darby canine kidney cells. *J. Cell Biol.* **146,** 313–320 (1999).
35. Füllekrug, J., Scheiffele, P. & Simons, K. VIP36 localisation to the early secretory pathway. *J. Cell Sci.* **112,** 2813–2821 (1999).
36. Dell'Angelica, E. C., Mullins, C. & Bonifacino, J. S. AP-4, a novel protein complex related to clathrin adaptors. *J. Biol. Chem.* **274,** 7278–7285 (1999).
37. Ladinsky, M. S., Kremer, J. R., Furcinitti, P. S., McIntosh, J. R. & Howell, K. E. HVEM tomography of the trans-Golgi network: structural insights and identification of a lace-like vesicle coat. *J. Cell Biol.* **127,** 29–38 (1994).
38. Ladinsky, M. S., Mastronarde, D. N., McIntosh, J. R., Howell, K. E. & Staehelin, L. A. Golgi structure in three dimensions: functional insights from the normal rat kidney cell. *J. Cell Biol.* **144,** 1135–1149 (1999).
39. Hedman, K., Goldenthal, K. L., Rutherford, A. V., Pastan, I. & Willingham, M. C. Comparison of the intracellular pathways of transferrin recycling and vesicular stomatitis virus membrane glycoprotein exocytosis by ultrastructural double-label cytochemistry. *J. Histochem. Cytochem.* **35,** 233–243 (1987).
40. Grindstaff, K. K. *et al.* Sec6/8 complex is recruited to cell–cell contacts and specifies transport vesicle delivery to the basal–lateral membrane in epithelial cells. *Cell* **93,** 731–740 (1998).
41. Mantei, N. *et al.* Complete primary structure of human and rabbit lactase-phlorizin hydrolase: implications for biosynthesis, membrane anchoring and evolution of the enzyme. *EMBO J.* **7,** 2705–2713 (1988).
42. Seed, B. An LFA-3 cDNA encodes a phospholipid-linked membrane protein homologous to its receptor CD2. *Nature* **329,** 840–842 (1987).
43. Harrison, P. T., Hutchinson, M. J. & Allen, J. M. A convenient method for the construction and expression of GPI-anchored proteins. *Nucleic Acids Res.* **22,** 3813–3814 (1994).
44. He, T. C. *et al.* A simplified system for generating recombinant adenoviruses. *Proc. Natl Acad. Sci. USA* **95,** 2509–2514 (1998).
45. Laemmli, U. K. Cleavage of structural proteins during the assembly of the head of bacteriophage T4. *Nature* **227,** 680–685 (1970).
46. White, J. *et al.* Rab6 coordinates a novel Golgi to ER retrograde transport pathway in live cells. *J. Cell Biol.* **147,** 743–759 (1999).
47. Diggle, P. J. *Statistical Snalysis of Spatial Point Patterns* (Academic, London, 1983).

ACKNOWLEDGEMENTS

We acknowledge Olympus and TILL Photonics for providing equipment and support to the Advanced Light Microscope Facility at EMBL; J. Rietdorf and R. Pepperkok for technical support; R. Tsien and G. Banting for ECFP and TGN38–EGFP cDNA, respectively; and N. LeBot and J. Füllekrug for GFP and gp27 antibodies, respectively. J. Ellenberg, G. Griffiths and R. Pepperkok are acknowledged for critical comments on the manuscript. P.K. was supported by a grant from the Max Plank Gesellschaft, D.T. by a Marie Curie Research grant, E.D. by a grant from the Secretaría de Estado de Educación, Universidades, Investigación y Desarollo, and K.S. by an EU network grant and a grant from the Deutsche Forschungsgemeinschaft. Correspondence and requests for materials should be addressed to K.S. Supplementary Information is available on http://www.mpi-cbg.de/content.php3?lang=en&aktID=videos8

© 2001 Macmillan Magazines Ltd